

## Direct excitation of dark plasmonic resonances under visible light at normal incidence†

Cite this: *Nanoscale*, 2014, 6, 2106

Yinghong Gu,<sup>a</sup> Fei Qin,<sup>a</sup> Joel K. W. Yang,<sup>bc</sup> Swee Ping Yeo<sup>a</sup> and Cheng-Wei Qiu<sup>\*a</sup>

Received 4th October 2013

Accepted 9th December 2013

DOI: 10.1039/c3nr05298b

[www.rsc.org/nanoscale](http://www.rsc.org/nanoscale)

Dark plasmon resonance modes are optical modes that have small scattering cross-sections and are thus difficult to excite directly by light at normal incidence. In this paper, we propose to excite quadrupolar and higher-order modes with normal incident light (in the visible regime) on a continuous plasmonic metallic surface covering a dielectric pillar array, hence resulting in narrow-band perfect absorption. Different from the general electromagnetic means of inducing dark modes, our dark modes are due to charge densities that are electrically induced by the standing-wave resonance of current on the thin metal sidewall of pillars. This new means of exciting dark modes can significantly improve the excitation efficiency and also provides an easy way to excite strong higher-order modes.

### Introduction

Dark plasmon resonances are charge oscillations localized on metal nanostructures that are weakly radiating and thus difficult to excite by light. In coupled plasmonic systems, these dark modes can be considered as a combination of multiple dipole resonances that collectively sum to zero.

The notable examples of dark modes reported in the literature include nanostructures arranged in dimers,<sup>1–3</sup> clusters,<sup>4–12</sup> rings or disks,<sup>13–16</sup> and dolmen<sup>10,17–20</sup> and stacked<sup>21–23</sup> geometries. In such configurations, the methods to excite dark modes utilize electron beams<sup>1,3,4,14</sup> and oblique incident light,<sup>13,15,16,24</sup> by inducing Fano resonances in asymmetric nanostructures<sup>25</sup> and asymmetric near-field environments,<sup>26</sup> or even in heterogeneous nanostructures at normal incidence,<sup>7,10–12,17,19–23,25,27</sup> which in general excite a bright dipole resonance first as the excitation source of the dark modes and thereby result in weak

absorption. One of the major characteristics of these dark modes is their narrowband resonances, enabling applications in refractive-index sensing and single-molecule sensing.<sup>11,12,15,20,25</sup> In the case of color filters and printing applications,<sup>28,29</sup> these narrowband features may lead to purer color selections. As most of these applications rely on the excitation of resonances by light at normal incidence, it is valuable to design structures that allow this form of illumination to also directly excite dark modes. In this work, we introduce an idealized design of a novel symmetry structure consisting of a continuous metal coating on dielectric nanopillars. Our analysis and numerical simulations of this structure show the presence of dark modes that can be effectively excited to produce perfect absorption of normally incident light.

Previously reported structures (consisting of metal nanodisks on dielectric nanopillars with a bottom backreflector plane) were shown to exhibit a broad range of colors<sup>28</sup> when viewed in reflection mode under bright-field illumination using an optical microscope. Reflectance peaks were observed at wavelengths corresponding to the dipole resonances of the nanodisks; changing the diameter of the nanodisks, and the interplay between resonances of the disk and the backreflector plane enabled a continuous tuning of the colors observed. In this letter, we demonstrate that a small modification of this structure results in a sharp reflectance dip in the spectra, overlaying the broader peaks in the original structure. By merely introducing a continuous 5 nm-thick Ag coating on the sidewalls of the nanopillars, the disk is in effect electrically shorted with the bottom backreflector layer. Reminiscent of the effects of conductive bridges across closely spaced metal structures,<sup>30,31</sup> our introduction of this conductive sidewall coating gives rise to new resonant modes. These resulting dark modes with quadrupole and higher-order multipoles are a consequence of the cancellation of the dipole of the nanodisk by dipoles of opposite polarity supported on the sidewalls, resulting in narrow-band perfect absorption. The metallic surface of this periodic pillar nanostructure is overall continuous. In contrast to the electromagnetically induced dark modes reported thus far in the

<sup>a</sup>Department of Electrical and Computer Engineering, National University of Singapore, Singapore 117576, Singapore. E-mail: [eleqc@nus.edu.sg](mailto:eleqc@nus.edu.sg)

<sup>b</sup>Institute of Materials Research and Engineering, Agency for Science, Technology and Research, 3 Research Link, Singapore 117602, Singapore

<sup>c</sup>Singapore University of Technology and Design, Engineering Product Development, Singapore 138682, Singapore

† Electronic supplementary information (ESI) available. See DOI: 10.1039/c3nr05298b

literature,<sup>10,13,16,17,22–24</sup> we present the following three contributions in this letter. Firstly, the dark modes are directly excited without the need for using induced bright mode; this markedly improves the excitation efficiency of dark modes. Secondly, our proposed scheme (of excitation with normal incidence on a continuous plasmonic metallic surface) can be regarded as an electrical resonant method to induce dark modes by creating and manipulating the electric charge on the shorting sidewalls where the electric current behaves as a standing wave; this is different from the other reported methods employing, for example, oblique incidence, stacked or planarized heterogeneous structures. Thirdly, owing to this slight but non-trivial modification on the sidewall, a broad-band highly reflective resonator is transformed into a narrow-band perfect absorber supporting quadrupole or even higher-order modes. Our proposed scheme may potentially find applications in sensing or color filters and printing.

## Results and discussion

Fig. 1a and b show our proposed structure comprising a periodic array of dielectric pillars that can be experimentally achieved *via* electron-beam lithography using a negative-tone hydrogen silsesquioxane (HSQ) resist on a Si substrate.<sup>28</sup> The structures are anisotropically covered by an Ag layer, and the thickness of the Ag layer on top of the HSQ pillars and the bottom layer is 15 nm, and the thickness of the Ag sidewall around the HSQ pillars is 5 nm (which is much thinner than the penetration depth of Ag under visible light). Since the thickness of the top/bottom Ag layer and the sidewall is different, a 2-step method is proposed to deal with the metal deposition (see ESI, Fig. S1†). Firstly, by using an electron-beam evaporator, a layer of silver can be deposited on the top of HSQ pillars and at the bottom,<sup>28</sup> which is similar to the structure in Fig. 1c and d, but the thickness of this

layer is about 10 nm. Secondly, another 5 nm Ag layer covering the whole structure (containing the top/bottom layer and the sidewall around pillars) can be added by Atomic Layer Deposition (ALD).<sup>32,33</sup> After that the Ag layer on top and bottom had increased to 15 nm and the sides of HSQ pillars are coated with 5 nm Ag sidewalls. Such a thin Ag sidewall allows the energy to flow into and out of the structure easily whilst still electrically connecting the top disks and bottom layer. This also makes our structure different from the pure metal pillars array<sup>34</sup> which blocks the electromagnetic wave outside the pillars.

Fig. 1e shows the reflection spectrum of a wave at normal incidence. For comparison purposes, we also include a similar structure of the same size but without the 5 nm Ag sidewall (Fig. 1c and d). For the structure without the Ag sidewall, there is a broadband peak in the visible light range (which has been discussed in detail in ref 28). In contrast, the reflectance of our proposed structure drops to nearly 0 at 600 nm. Given that the structures sit on a Si substrate, the transmittance of the structure can effectively be neglected and the reflectance dip thus indicates absorbance instead. Hence, the thin Ag sidewall coating transforms this structure from a broad-band reflector to a narrow-band near-perfect absorber.

For the reflection spectrum, the broad-band peak of the structure portrayed in Fig. 1c and d results from the coupling of the Ag disks on top of the HSQ pillars and the Ag bottom layer on the substrate. However, the Ag sidewall serves as a bridge connecting the top disks and the bottom layer, and the top disks thus cannot be regarded as simple dipoles. As can be seen from the plots in Fig. 2a depicting the charge distribution at resonance, the charge can be pumped into the sidewall by the resonance of the top disk and a plasmonic standing wave will then be generated along the sidewall.

The charge is accumulated at the edge of the top disk while remaining zero at the bottom. At the antinode of the standing

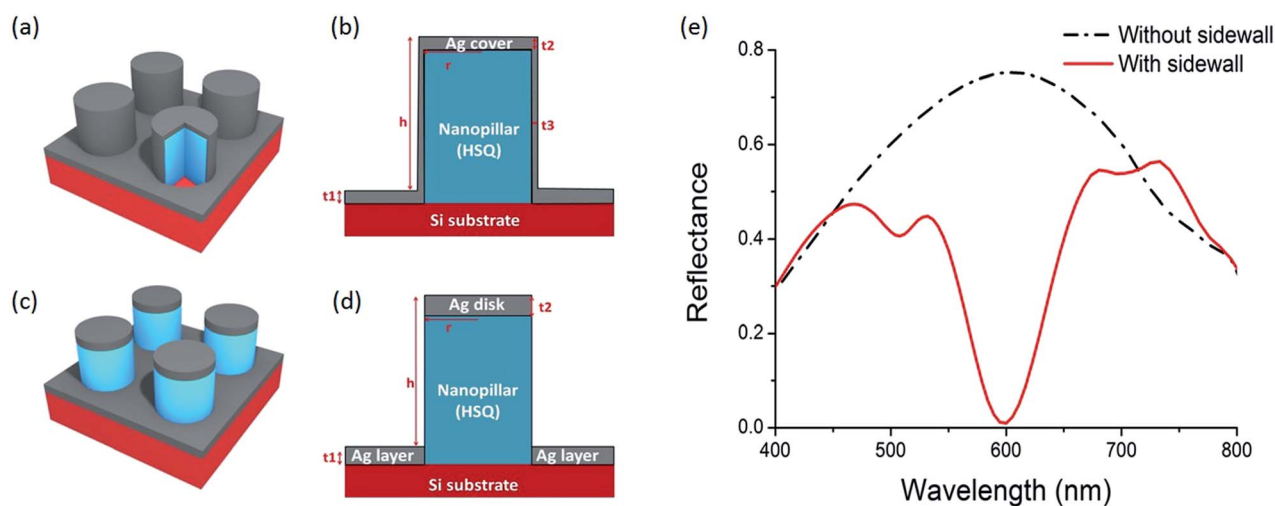


**Fig. 1** (a) Schematic diagram of the periodic HSQ pillars covered by a Ag layer structure. (b) A cross-sectional view of the unit cell in (a),  $t_1 = t_2 = 15$  nm,  $t_3 = 5$  nm,  $r = 50$  nm. (c) Schematic diagram of the periodic HSQ pillars without Ag sidewalls. (d) A cross-sectional view of the unit cell in (c),  $t_1 = t_2 = 15$  nm,  $r = 45$  nm. (e) The reflection spectrum of the structure with a Ag sidewall (shown in a and b) and without a sidewall (shown in c and d),  $h = 85$  nm,  $p = 120$  nm,  $p$  is the period of the unit cell,  $h$  is the height of the pillar from the Ag bottom layer, and  $g$  is the gap between two neighbouring pillars,  $p = 2r + g$ .

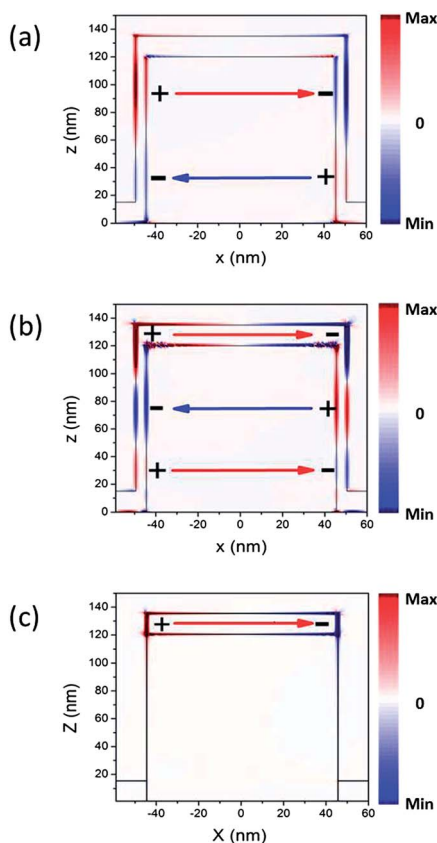


Fig. 2 Higher-order dark modes excited by visible light. (a) The charge distribution for an excited quadrupolar dark mode at a wavelength of 600 nm, with  $h = 120$  nm,  $p = 120$  nm. (b) The charge distribution for a hexapolar dark mode at a wavelength of 569 nm, with  $h = 120$  nm,  $p = 120$  nm. (c) For comparison, the charge distribution for bright dipole mode resonance of the structure without a sidewall shown in Fig. 1c and d. The signs and arrows denote dipoles and their directions. It should be pointed out that some of the area with extremely large charge density has been smoothed; the highest intensity has been suppressed in order to maintain the contrast.

wave in the middle of the sidewall, however, charge is accumulated and forms another dipole in the middle of the sidewall; this is opposite to the dipoles of the top disks and the charge profile on the metal covering the pillar and thus constitutes a quadrupole (dark mode) where the two sets of dipole moment nullify each other and the radiation is reduced to yield zero reflection of the structure. Different from the dark modes reported for plasmonic oscillators (*e.g.* in nanoparticles or nanorods<sup>5–12,17–23</sup>) caused by the coupling of the electromagnetic field, this dark mode in the continuous metal structure is caused by the electric current oscillation and charge accumulation driven by the bright dipole resonance of the top disk. Seen from this perspective, we can regard it as electronically induced absorption (in contrast to electromagnetically induced absorption).

In addition, we observe in Fig. 1e a minor dip at a shorter wavelength for the reflectance of our proposed structure. This is due to the same effect as explained above, but with a hexapolar mode on the sidewall of the pillar. At a wavelength of 508 nm,

two more dipoles (other than the one on the top disk) are induced on the sidewall and so each pillar is effectively holding a hexapole also in dark mode, with a form of “positive–negative–positive” distribution. These high-order multipolar dark modes are suppressing the radiation and reducing the reflectance as well. In Fig. 1e, this hexapolar mode is much weaker than the quadrupolar mode because the resonance wavelength of the hexapolar mode is far away from that of the top disk dipoles for the structure without the sidewall while the resonance wavelength of the quadrupolar mode is close to it. The dark modes are mainly induced by the top disk dipoles; hence, only the dark modes near the top-disk dipole resonance wavelength can be so strong. If we open a ring gap on the sidewall at the position where the charge is accumulated and the electric current is zero, the quadrupolar and high-order multipolar modes will not be affected and the spectrum near the resonance will remain almost the same; this device can be regarded as an optical flute which can absorb specific wavelengths (similar to the flute playing specific tones).

To further investigate how the structure performs as a perfect absorber, we plot the profiles of the electric field, Poynting vectors and electric current in Fig. 3 for both quadrupolar and hexapolar modes to explain the energy absorption. From the electric field plots, we can readily determine the positions of the quadrupole and hexapole; since the entire structure has a continuous Ag cover, the power flow is squeezed into the gaps between the pillars. When the incident wavelength is at the quadrupolar mode resonance, the power flow penetrates through the Ag sidewall at the position of zero net charge and then exits at the bottom, encircling the charge like a vortex. Each time the power passes the sidewall, a large amount of energy is lost. Hence, the power flow is localized along the sidewall (either in or out of the pillar) and then energy is lost on the sidewall. Interestingly, if the pillar is made of pure silver without the HSQ core, power flow cannot freely go inside and outside the pure silver pillars and light is thus mostly reflected. For our structure, the sidewall is thin enough for light to penetrate, which drives the power flow to encircle and flow around the accumulated charge, generating the energy vortices along the sidewall of the pillars; it thus leads to greatly increased absorbance. A similar phenomenon can be observed for the hexapolar mode, where the charge on the silver sidewall enforces the power flow to go “in–out–in” the pillar. Since we presume that our structure has only one type of loss (*i.e.* metallic loss in silver), all of the absorption should take place in the silver cover and the energy lost in silver is proportional to the square of the electric current density. We observe from the electric current distributions for different multipoles shown in Fig. 3e–g that most of the energy is depleted on the sidewall at the resonance wavelength. Hence, energy is mostly lost on the sidewall instead of the top disks or the bottom layer.

Fig. 3 allows us to infer how each part of the structure works. The top metal disks, if separated from the other parts of the structure, can clearly be regarded as dipole resonators. However, once the thin metal sidewall is connected, the dipole mode no longer holds and the disk performs like a pump pushing the current into the sidewall. We should thus focus on

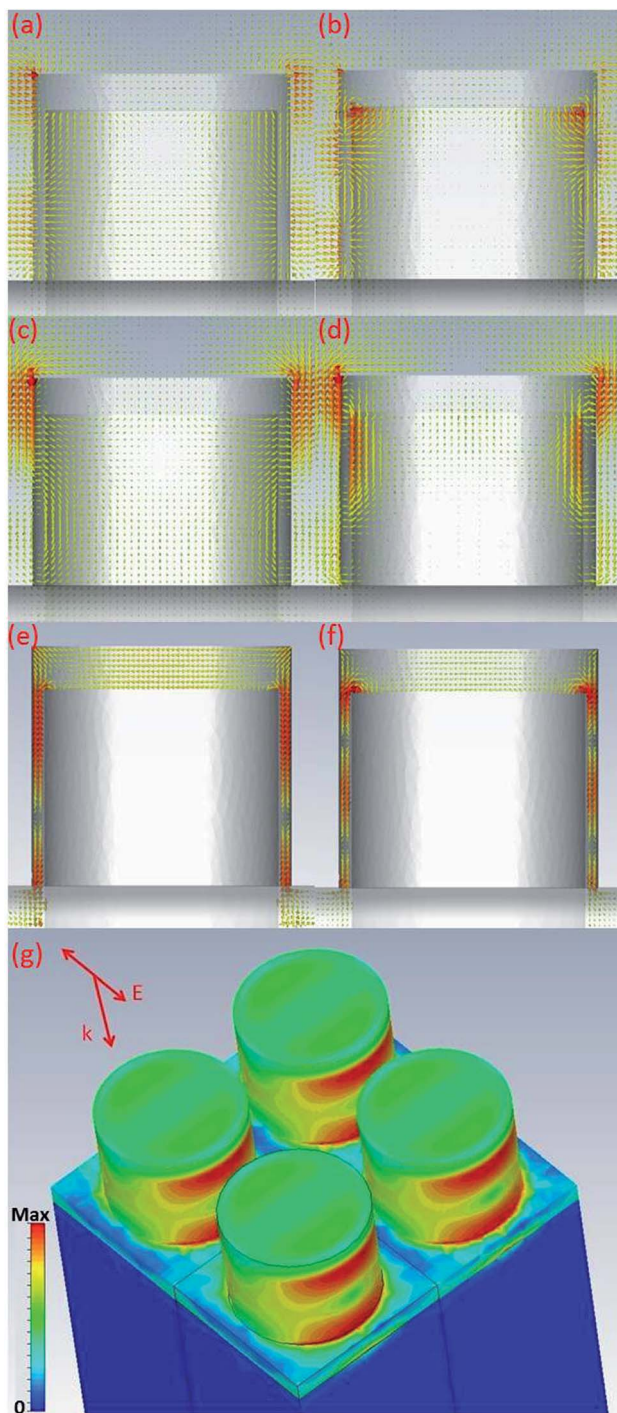


Fig. 3 The electric-field distribution of (a) quadrupolar mode and (b) hexapolar mode. The Poynting vector distribution of (c) quadrupolar mode and (d) hexapolar mode. The electric current distribution in Ag of (e) quadrupolar mode and (f) hexapolar mode. (g) 3D view of the electric-current intensity profile in log scale at quadrupolar mode; it can also indicate the energy absorption profile in which most energy is absorbed at the sidewall (dissipated energy  $E \propto J^2$ ). For the structure,  $h = 85$  nm,  $p = 120$  nm. Both the size and the color of the arrow show the magnitude, and all intensity is normalized.

the 5 nm silver sidewall when exciting dark modes. Firstly, it electrically breaks the bright dipole mode on the disks so that there are only directly excited dark mode resonances in our

structure (Fig. 2a and b); this is quite different from previous research on dolmen or stacked structures that utilize a bright dipole mode to excite the dark modes. Secondly, the sidewall performs as the carrier of the standing wave; our dark modes are electrically (instead of electromagnetically) induced such that it needs the metal sidewall to support the current oscillation. Lastly, the sidewall is also the energy consumer; the quadrupoles or higher-order multipoles guide the power to penetrate such a thin metal layer again and again (Fig. 3c and d) and the energy is greatly depleted each time the power passes the sidewall (Fig. 3g). We infer from Fig. 3e and f that the electric current on the bottom layer is so small that we can effectively disregard it, thus implying that this silver layer is not an important part of the structure. Indeed, it is not necessary for supporting the standing wave on the sidewall and the incident light can hardly reach the bottom. Without this bottom layer, FDTD simulations likewise yield the narrowband absorption associated with the dark modes in the reflection spectrum.

In addition to using directly excited quadrupolar dark mode to achieve perfect absorption, we can equally seek to enhance the hexapolar mode so as to make this structure a dual-band near-perfect absorber targeting particular wavelengths. We infer from Fig. 4 that the resonance wavelength and absorptance depend on the height  $h$  of the pillar. The red and green lines plotted in Fig. 4 correspond to the quadrupole and hexapole resonances, respectively. The resonance wavelength is almost linear with  $h$ , and the slopes of both resonance wavelengths are approximately 2. When  $h$  is small, the high-order modes, such as hexapole mode, are not strong enough to be observed. The hexapolar mode can be easily observed when  $h$  exceeds 85 nm. As  $h$  becomes larger, it is easier to accommodate and enhance higher-order multipolar modes; for example, we observe from Fig. 4a that at  $h = 115$  nm the absorption of the hexapolar mode is even more significant than that of the quadrupolar mode. It can be understood that the results show that the higher structures can support stronger hexapole modes, and when  $h$  is small, the hexapole mode becomes extremely weak. Although the dark mode resonances are located on the sidewall, they still need the top disk to drive the charge into sidewall. Therefore, the dark modes, no matter quadrupole or hexapole, will become weaker as they shift further away from the original resonance of the disk (about 600 nm, shown by the black dashed curve in Fig. 1e, which is the resonance peak for nanostructures without sidewalls). When  $h$  is small, the resonance wavelength of hexapole mode would be so short, as the trend shown in Fig. 4b, that the amount of charge pumped into the sidewall by the top disk would be very limited and the dark mode resonances would be too weak to be observed.

In fabrication, it is very difficult to achieve a 5 nm homogeneous silver sidewall and accurately control its thickness. By silver evaporation, the layer may be not continuous or even patchy. So the sidewall is proposed to be deposited by ALD, but the thickness is still hard to keep uniform at such small size. To address this limitation, we also need to investigate whether this structure can tolerate variations in the sidewall thickness. Additional simulations have been performed in Fig. 4c to examine how the absorption (shown by reflectance) at the

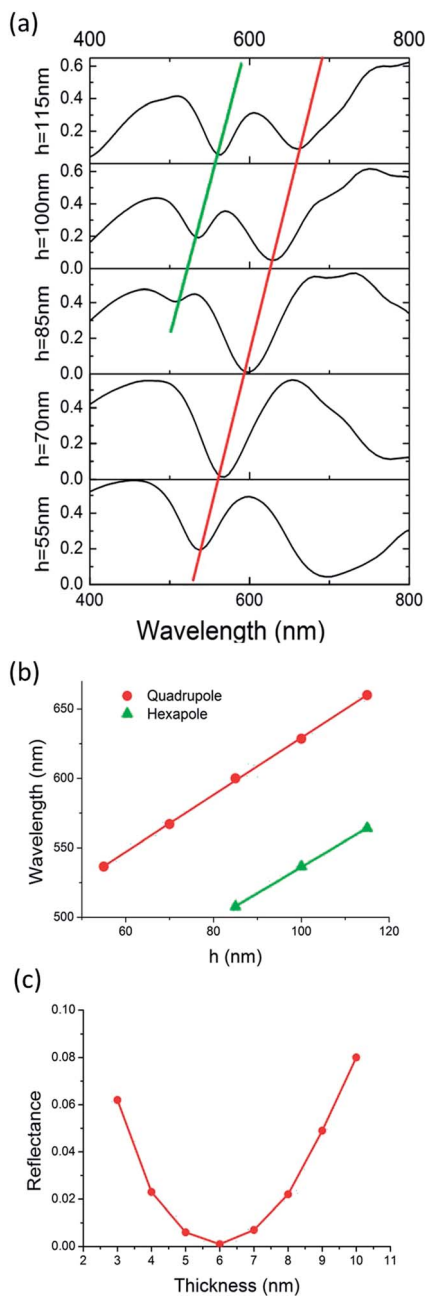


Fig. 4 (a) The reflection spectrum of the structure with different  $h$ , where the red and green lines indicate quadrupolar and hexapolar modes respectively. (b) The fitting of the resonance wavelength versus  $h$  for quadrupolar and hexapolar modes (with slope of 2.06 and 1.88 respectively). (c) The reflectance of the quadrupole resonance dip for the structure with different Ag sidewall thicknesses, with fixed HSQ height  $h = 85\text{ nm}$ , period  $p = 120\text{ nm}$ .

quadrupole resonance dip depends on the thickness of the Ag sidewall. The simulation results in Fig. 4c affirm that reflectance can be kept below 10% even when the thickness varies from 3 nm to 10 nm.

Another way to reduce the fabrication difficulty is to simplify the 2-step silver deposition method into just an ALD process. After achieving the HSQ pillar array by EBL, the silver evaporation process can be skipped, and a thin silver cover can be

directly deposited on the structure by ALD. As a consequence, the top layer and sidewall will have the same thickness ( $t_1 = t_2 = t_3$  in Fig. 1b). This simplified structure can still support the dark modes, but the strength of the mode is greatly reduced (shown in ESI, Fig. S2†). As discussed before, the sidewall should be thin enough to let the power flow penetrate into the pillar, while the top disks should be thick enough to prevent the power flow from directly going inside and guide the power flow into the gaps (see Fig. 3c and d). Thus, the Ag cover with the same thickness cannot satisfy both requirements perfectly at the same time, and the efficiency of dark mode excitation is reduced.

## Conclusions

In summary, we have proposed a new mechanism to directly excite dark modes (including the fundamental and higher-order modes) by using an electrical shorting approach with a continuous metal cover on a periodic HSQ pillar template. Such an approach is quite different from the classical (indirect) methods of introducing dark modes (which are usually of fundamental order). Owing to the high efficiency of direct excitation, our mechanism and nanosurface can additionally be naturally employed to achieve narrow-band perfect absorption under visible light. The top metal disks behave like an electric current generator, and the quadrupoles and high-order multipoles in the dark modes can be excited on the sidewall electrically. At the resonance wavelength, the reflectance can be almost zero and the bandwidth is around 70 nm. Furthermore, by manipulating the structure size, we can also enhance the hexapolar mode to make it a dual-band absorber. Apart from the obvious application as an absorber, our proposed method of exciting the dark mode in an electrically continuous structure may find applications in many other optical devices.

## Method

The reflection spectra and distribution of electric charge in Fig. 1e, 2 and 4 were generated by means of LUMERICAL, a commercial finite-difference time-domain (FDTD) code. A plane wave polarized along the  $x$ -axis was used as incidence. The distributions of the electric field, Poynting vector and current density in Fig. 3 were calculated with CST MICROWAVE STUDIO software based on the finite integration technique (FIT). The electric permittivity of silver is taken from the material of “Ag (Silver) – Palik (0–2  $\mu\text{m}$ )” from LUMERICAL database.

## Acknowledgements

J.K.W.Y. would like to acknowledge funding support from the Agency for Science, Technology and Research (A\*STAR) Young Investigatorship (grant number 0926030138), SERC (grant number 092154099), and National Research Foundation grant award No. NRF-CRP 8-2011-07. C.W.Q. acknowledges financial support from Grant R-263-000-688-112 from the National University of Singapore.

## Notes and references

- 1 H. Duan, A. I. Fernández-Domínguez, M. Bosman, S. A. Maier and J. K. W. Yang, *Nano Lett.*, 2012, **12**(3), 1683–1689.
- 2 P. Nordlander and C. Oubre, *Nano Lett.*, 2004, **4**(5), 899–903.
- 3 M. W. Chu, V. Myroshnychenko, C. Chen, J. P. Deng, C. Y. Mou and F. J. García de Abajo, *Nano Lett.*, 2009, **9**(1), 399–404.
- 4 F. Wen, J. Ye, N. Liu, P. V. Dorpe, P. Nordlander and N. J. Halas, *Nano Lett.*, 2012, **12**(9), 5020–5026.
- 5 J. Ye, F. Wen, H. Sobhani, J. B. Lassiter, P. V. Dorpe, P. Nordlander and N. J. Halas, *Nano Lett.*, 2012, **12**(3), 1660–1667.
- 6 Y. Zhang, F. Wen, Y. Zhen, P. Nordlander and N. J. Halas, *Proc. Natl. Acad. Sci. U. S. A.*, 2013, **110**, 239215.
- 7 M. Rahmani, D. Y. Lei, V. Giannini, B. Lukiyanchuk, M. Ranjbar, T. Y. F. Liew, M. Hong and S. A. Maier, *Nano Lett.*, 2012, **12**(4), 2101–2106.
- 8 M. Hentschel, D. Dregely, R. Vogelgesang, H. Giessen and N. Liu, *ACS Nano*, 2011, **5**(3), 2042–2050.
- 9 J. A. Fan, C. Wu, K. Bao, J. Bao, R. Bardhan, N. J. Halas, V. N. Manoharan, P. Nordlander, G. Shvets and F. Capasso, *Science*, 2010, **28**, 1135.
- 10 P. A. Gonzalez, M. Schnell, P. Sarriugarte, H. Sobhani, C. Wu, N. Arju, A. Khanikaev, F. Golmar, P. Albella, L. Arzubia, F. Casanova, L. E. Hueso, P. Nordlander, G. Shvets and R. Hillenbrand, *Nano Lett.*, 2011, **11**(9), 3922–3926.
- 11 J. A. Fan, Y. He, K. Bao, C. Wu, J. Bao, N. B. Schade, V. N. Manoharan, G. Shvets, P. Nordlander, D. R. Liu and F. Capasso, *Nano Lett.*, 2011, **11**(11), 4859–4864.
- 12 J. A. Fan, K. Bao, C. Wu, J. Bao, R. Bardhan, N. J. Halas, V. N. Manoharan, G. Shvets, P. Nordlander and F. Capasso, *Nano Lett.*, 2010, **10**(11), 4680–4685.
- 13 F. Hao, E. Larsson, T. Ali, D. Sutherland and P. Nordlander, *Chem. Phys. Lett.*, 2008, **458**, 262–266.
- 14 F. P. Schmidt, H. Ditlbacher, U. Hohenester, A. Hohenau, F. Hofer and J. R. Krenn, *Nano Lett.*, 2012, **12**(11), 5780–5783.
- 15 F. Hao, Y. Sonnefraud, P. V. Dorpe, S. A. Maier, N. J. Halas and P. Nordlander, *Nano Lett.*, 2008, **8**(11), 3983–3988.
- 16 Y. Sonnefraud, N. Verellen, H. Sobhani, G. A. E. Vandenbosch, V. V. Moshchalkov, P. V. Dorpe, P. Nordlander and S. A. Maier, *ACS Nano*, 2010, **4**(3), 1664–1670.
- 17 S. Zhang, D. A. Genov, Y. Wang, M. Liu and X. Zhang, *Phys. Rev. Lett.*, 2008, **101**, 047401.
- 18 J. Gu, R. Singh, X. Liu, X. Zhang, Y. Ma, S. Zhang, S. A. Maier, Z. Tian, A. K. Azad, H. T. Chen, A. J. Taylor, J. Han and W. Zhang, *Nat. Commun.*, 2012, **3**, 1151.
- 19 N. Verellen, Y. Sonnefraud, H. Sobhani, F. Hao, V. V. Moshchalkov, P. V. Dorpe, P. Nordlander and S. A. Maier, *Nano Lett.*, 2009, **9**(4), 1663–1667.
- 20 C. Wu, A. B. Khanikaev, R. Adato, N. Arju, A. A. Yanik, H. Altug and G. Shvets, *Nat. Mater.*, 2012, **11**, 69.
- 21 A. Artar, A. Yanik and H. Altug, *Nano Lett.*, 2011, **11**(4), 1685–1689.
- 22 R. Taubert, M. Hentschel, J. Kästel and H. Giessen, *Nano Lett.*, 2012, **12**(3), 1367–1371.
- 23 N. Liu, L. Langguth, T. Weiss, J. Kästel, M. Fleischhauer, T. Pfau and H. Giessen, *Nat. Mater.*, 2009, **8**, 758–762.
- 24 F. Schertz, M. Schmelzeisen, R. Mohammadi, M. Kreiter, H. J. Elmers and G. Schonhense, *Nano Lett.*, 2012, **12**(4), 1885–1890.
- 25 J. Zhao, C. Zhang, P. V. Braun and H. Giessen, *Adv. Mater.*, 2012, **24**, 247–252.
- 26 Z.-G. Dong, H. Liu, M.-X. Xu, T. Li, S.-M. Wang, J.-X. Cao, S.-N. Zhu and X. Zhang, *Opt. Express*, 2010, **18**(21), 22412.
- 27 B. Lukiyanchuk, N. I. Zheludev, S. A. Maier, N. J. Halas, P. Nordlander, H. Giessen and C. T. Chong, *Nat. Mater.*, 2010, **9**(9), 707–715.
- 28 K. Kumar, H. Duan, R. S. Hegde, S. C. W. Koh, J. N. Wei and J. K. W. Yang, *Nat. Nanotechnol.*, 2012, **7**, 557–561.
- 29 T. Ellenbogen, K. Seo and K. B. Crozier, *Nano Lett.*, 2012, **12**(2), 1026–1031.
- 30 F. Ye, M. J. Burns and M. J. Naughton, *Nano Lett.*, 2013, **13**(2), 519–523.
- 31 B. Abasahl, S. D. Gupta, C. Santschi and O. J. F. Martin, *Nano Lett.*, 2013, **13**(9), 4575–4579.
- 32 M. Kariniemi, J. Niinisto, T. Hatanpää, M. Kemell, T. Sajavaara, M. Ritala and M. Leskelä, *Chem. Mater.*, 2011, **23**(11), 2901–2907.
- 33 A. Niskanen, T. Hatanpää, K. Arstila, M. Leskelä and M. Ritala, *Chem. Vap. Deposition*, 2007, **13**(8), 408–413.
- 34 K. Wang, E. Schonbrun, P. Steinvurzel and K. B. Crozier, *Nat. Commun.*, 2011, **2**, 469.